Excitons and exciton confinement in crystalline organic thin films grown by organic molecular-beam deposition

E. I. Haskal,* Z. Shen, P. E. Burrows, and S. R. Forrest
Advanced Technology Center for Photonics and Optoelectronic Materials, Department of Electrical Engineering, Princeton University, Princeton, New Jersey 08544
(Received 25 August 1994)

We study excitons in thin films of varying thickness of two organic molecular crystals grown by the ultrahigh-vacuum process of organic molecular-beam deposition; 3,4,9,10-perylenetetracarboxylic dianhydride (PTCDA), and 3,4,9,10-perylenetetracarboxylic bis-benzimidazole (PTCBI). By using electroabsorption spectroscopy, low-temperature fluorescence, and absorption techniques, we find that nearly spatially symmetric charge-transfer/Wannier-like excitons are present in crystalline PTCDA films, and that these excitons can be confined in multilayer stacks of ultrathin layers of thicknesses ranging from 10 to 100 Å. In PTCBI films, however, the exciton has a smaller radius, and thus much weaker spectral and electric-field dependences on layer thickness are observed. In addition, we present theoretical and experimental evidence showing that exciton-lattice interactions may be modified by the growth of ultrathin layers and the subsequent confinement of the charge-transfer excitons.

I. INTRODUCTION

The nature of excitons in organic molecular crystals (OMC's) has been the subject of intense debate for over thirty years.[1] In particular, molecular excitons have been described as either Frenkel or charge-transfer (CT) states.[2] A Frenkel exciton is a correlated electron-hole pair that is localized on the same molecular site, where the orbit of the electron in the excited state is smaller than the molecular separation in the crystal. For the case of the CT exciton, the electron is correlated with a hole located at a neighboring molecular site. Therefore, CT excitons resemble both Frenkel and Wannier excitons common in inorganic systems, where the interaction energy between atomic cores is large and the radius of the exciton is often more than an order of magnitude greater than the interatomic separation.

Because of the small oscillator strength of direct CT transitions from the ground state,[3] it has been difficult to observe the existence of CT excitons using standard absorption techniques. However, through the use of electric-field-modulated reflectance[4] and electroabsorption spectroscopy,[5] CT transitions have been observed in several OMC's. In addition, it has been shown that calculation of the energies of higher-order CT states in these materials only had to account for the spatially averaged dielectric constant of the crystal, rather than the anisotropic dielectric tensor characteristic of most OMC's.[6] The presence of these spatially extended Wannier-like/charge-transfer excitons in certain OMC's has been most directly demonstrated using electroabsorption spectroscopy,[5,7] where the distinction between the linear Stark effect and polarization (or CT) effects in OMC's may be independently determined by analysis of the first and second derivatives, respectively, of the absorption with respect to the photon energy.

More recently, the development of the ultrahigh-vacuum process of organic molecular-beam deposition (OMBD) (Ref. 8) has allowed for the growth of multilayer stacks of ultrathin (10–500 Å) layers of the closely stacked, strongly π-bonded crystalline organic material 3,4,9,10-perylenetetracarboxylic dianhydride (PTCDA) spatially separated by layers of 3,4,7,8-naphthalenetetracarboxylic dianhydride (NTCDA).[9] It was found that decreasing the PTCDA layer thickness from 500 to 10 Å results in blueshifts of the PTCDA absorption peaks, an increase in the fundamental ground-state vibrational frequency, and a redistribution of fluorescence intensity to higher energy.[10] These observations have been attributed to the confinement of PTCDA excitons with a radius of 12 Å (or 3–4 molecules) in these spatially restricted geometries.[9]

In this work, we use several spectroscopic techniques to investigate the optical properties of excitons in bulk thin films (1000 Å thick) and in ultrathin layers (10–500 Å thick) of two closely related, planar organic molecules; namely, PTCDA and 3,4,9,10-perylenetetracarboxylic bis-benzimidazole (PTCBI). We find from electroabsorption measurements that the lowest-energy exciton observed in PTCDA is nearly spatially symmetric, with a radius of ~13 Å. In PTCBI, however, the exciton has a much smaller CT component, and therefore a smaller radius. These results are corroborated by analysis of the fluorescence and absorption spectra of multilayer stacks comprised of ultrathin layers of combinations of these molecules. We observe spectral changes due to confinement of the spatially extended PTCDA exciton in layers thinner than 100 Å, whereas these effects are not observed for the smaller-radius excitons in PTCBI. In addition, we present a quantitative analysis of the modification of exciton-lattice interactions in ultrathin layers of OMC's such as PTCDA which are characterized by a strong exciton-phonon coupling.

We begin in Sec. II with a description of the lattice

0163-1829/95/51(7)/4449(14)/$06.00

structures of both PTCDA and PTCBI as characterized by x-ray and reflection high-energy electron diffraction (RHEED). Film growth using OMBD is described in Secs. III and IV. In Sec. III, we probe the nature of excitons in OMBD-grown bulk PTCDA and PTCBI films through the use of electroabsorption (EA) spectroscopy. By fitting the EA spectra to a simple theory, we determine the radius and relative Wannier and CT content of the lowest-energy observed exciton in these materials, as well as determine the effects of crystal anisotropy on the exciton. In Sec. IV, we describe the effects of confinement of excitons in ultrathin layers of PTCDA or PTCBI separated by layers of NTCDA. An analysis of the experimental results is presented in Sec. V, leading to a discussion in Sec. VI of the nature of exciton-phonon coupling in these materials. Conclusions are presented in Sec. VII.

II. MATERIALS AND GROWTH

Figure 1 shows the structural formulas and two views of the unit cell for bulk crystals of PTCDA and PTCBI as characterized by x-ray diffraction. These two compounds and NTCDA crystallize in the same monoclinic lattice structure (space group $P2_1/c$) with lattice parameters listed in Table I. As can be seen in Fig. 1, both PTCDA and PTCBI form in stacked molecular structures; however, the interplanar stacking distance of PTCDA molecules is 3.21 Å, as compared to 3.45 Å for PTCBI.

The unusually small interplanar stacking distance in PTCDA leads to a large π-orbital overlap between the planar molecules in the stacking direction. This large overlap results in hole mobilities of ~ 1 cm^2/V s, and a total bandwidth of ~ 0.9 eV,[12] where the bandwidth is defined as the sum of the widths of the highest occupied molecular orbital (HOMO) band and the lowest unoccupied molecular orbital (LUMO) band. In addition, the effects of the crystal anisotropy are manifested in the dielectric constant[13] (where for PTCDA $\varepsilon_{\parallel}/\varepsilon_{\perp} > 2$, with the subscripts $\parallel$ and $\perp$ referring to the directions parallel to the film plane and in the stacking direction, respectively), refractive index[13] (where $n_{\parallel}/n_{\perp} > 1.4$) and electrical conductivity[12] ($\sigma_{\parallel}/\sigma_{\perp} < 10^{-6}$). Thus, parallel to the film plane, PTCDA exhibits intermolecular interactions typically observed in most OMC's, whereas in the stacking direction its electronic properties bear similarities to both inorganic and organic semiconductors. In contrast to PTCDA, the larger interplanar stacking distance of PTCBI leads to a considerably reduced π-orbital overlap and electronic anisotropy. Thus, although these materials are very similar in composition, we expect that their excitonic (and hence spectral) properties will be considerably different. By investigation of these differences, we can understand in greater depth the nature of excitons in closely packed OMC's as well as in the more common, loosely coupled OMC's.

TABLE I. Lattice unit cell parameters for bulk crystals.

Lattice parameters	PTCDA	PTCBI	NTCDA
a (Å)	3.719	4.749	7.888
b (Å)	11.96	8.880	5.334
c (Å)	17.34	28.24	12.74
β (°)	98.81	100.16	109.04
Reference	11	This work	11

Prior to loading into the OMBD growth chamber,[14] commercially available[15] PTCDA and NTCDA, as well as PTCBI synthesized following previously published methods,[16] were each purified in three successive cycles using thermal gradient sublimation.[17] Typical vacuum sublimation temperatures for PTCDA, PTCBI, and NTCDA are 400 °C, 425 °C, and 210 °C, respectively. The

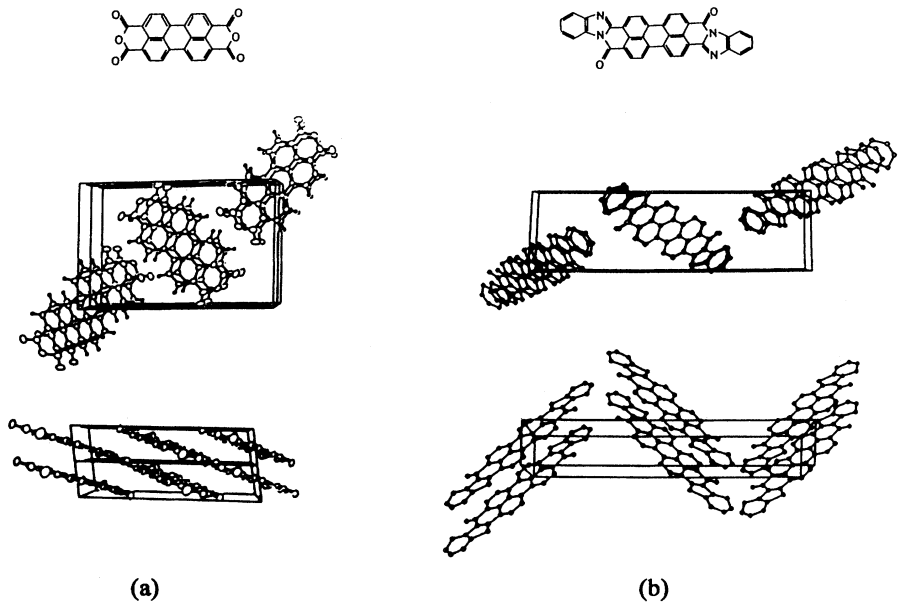

FIG. 1. Structural formulas and two perspective views of the bulk unit cells of (a) PTCDA and (b) PTCBI.

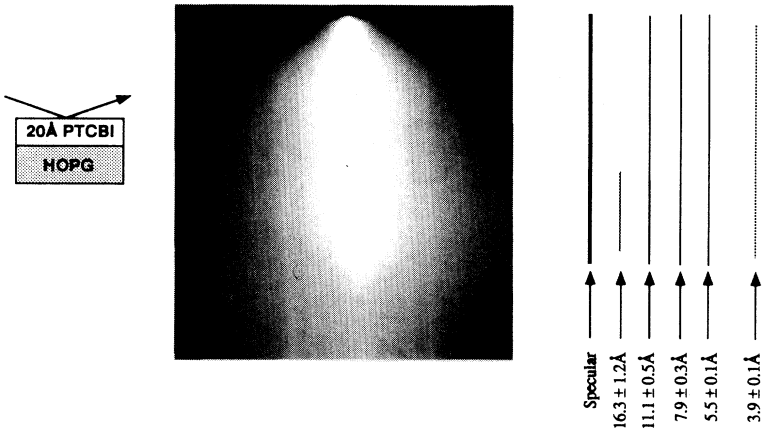

FIG. 2. Reflection high-energy electron-diffraction pattern of an OMBD-grown 20 Å PTCBI layer on highly oriented pyrolitic graphite. Streaks are labeled with their corresponding lattice dimensions.

synthesis and purification of PTCBI produced crystalline whiskers of a mixture of its two isomers, where the imidazole group was in either the *cis* or *trans* position (Fig. 1).

It has previously been observed that ordered thin films of crystalline organic materials may be deposited over large surface areas on incommensurate substrates using OMBD.[8,14,18] In those experiments, grazing-incidence x rays and *in situ* RHEED were used to show that OMBD resulted in a layer-by-layer growth of PTCDA,[18] with layer thicknesses uniform to within one monolayer for all samples. To confirm that the ordered growth of PTCBI occurs in a manner similar to PTCDA,[19] Fig. 2 shows a typical RHEED pattern for a 20 Å thick layer of PTCBI grown at ~90 K on highly oriented pyrolitic graphite. Note that the RHEED streaks are long and continuous, implying that the organic film surface is flat and crystalline, with no island overgrowth. This result is consistent with previous data showing that "quasiepitaxial" crystalline films can be grown on a wide variety of incommensurate substrates due to weak coupling between the deposited film and the substrate.[20] Therefore the OMBD growth of crystalline organic thin films of PTCDA and PTCBI on glass substrates, as well as in organic multilayer stacks, produces highly ordered layers which are suitable for the investigation of their fundamental optical and electronic properties.

III. ELECTROABSORPTION SPECTRA OF EXCITONS IN BULK THIN FILMS

It has previously been shown[5,21] that by fitting the EA spectrum to a simple theory it is possible to determine the relative importance of the Wannier and CT types of excitons in OMC's. In addition, by measuring the EA spectra for electric fields oriented along two orthogonal crystalline axes, it is possible to determine the effects of crystalline anisotropy on the exciton states.

An exciton eigenstate responds to an electric field via the Stark shift of its absorption line as well as via line broadening. Let ψ_i be the exciton state with energy E_i at zero applied field ($\mathbf{F}=\mathbf{0}$). The Stark shift of state ψ_0 (with energy E_0) is given by

$$\langle \Delta E \rangle = \sum_{i \neq 0} \frac{|\langle \psi_0 | q\mathbf{F}\cdot\mathbf{r} | \psi_i \rangle|^2}{E_0 - E_i} , \tag{1}$$

where q is the electronic charge and $\mathbf{r}$ is the displacement vector of electron and hole. Similarly, the line broadening is given by

$$\langle (\Delta E)^2 \rangle = \langle \psi_0 | (q\mathbf{F}\cdot\mathbf{r})^2 | \psi_0 \rangle . \tag{2}$$

Assuming that the change in absorption coefficient ($\Delta\alpha$) with respect to energy due to the applied field is small, then

$$\Delta\alpha = \frac{d\alpha}{dE}\langle \Delta E \rangle + \frac{1}{2}\frac{d^2\alpha}{dE^2}\langle (\Delta E)^2 \rangle + \cdots . \tag{3}$$

The quadratic field dependence of both $\langle \Delta E \rangle$ and $\langle (\Delta E)^2 \rangle$ in Eq. (3) implies that $\Delta\alpha$ is proportional to the square of the applied electric field.

To estimate $\langle \Delta E \rangle$ and $\langle (\Delta E)^2 \rangle$, and to explain the relative magnitude of the EA in two orthogonal crystalline directions, we first investigate the influence of crystal anisotropy on the EA spectrum. We begin with a study of the EA in thin films of PTCDA grown on glass, where the planar molecules form stacks tilted at 10°–12° from the substrate normal.[22] With this small tilt angle, we infer that fields applied along the substrate normal are approximately aligned parallel to the stacks (the z direction), whereas the in-plane fields are aligned parallel to the molecular planes. Due to the anisotropic crystal structure described in Sec. II, we must take the anisotropy of effective mass (m^*) into account by writing the Hamiltonian as

$$H = -\frac{\hbar^2}{2}\left[\frac{1}{m_{\parallel}^*}\left(\frac{\partial^2}{\partial x^2}+\frac{\partial^2}{\partial y^2}\right)+\frac{1}{m_{\perp}^*}\frac{\partial^2}{\partial z^2}\right] + V_{\text{Coul}} + q\mathbf{F}\cdot\mathbf{r} , \tag{4}$$

where $\hbar$ is Planck's constant divided by 2π, $m_{\parallel}^*$ and $m_{\perp}^*$ are the reduced effective masses parallel and normal to the film plane, and V_{Coul} is the Coulomb potential. Changing the coordinates to $\bar{x}=x\sqrt{m_{\parallel}^*/m_{\perp}^*}$, $\bar{y}=y\sqrt{m_{\parallel}^*/m_{\perp}^*}$, and $\bar{z}=z$, the Stark field term is then

$$q\mathbf{F}\cdot\mathbf{r}=q[\bar{z}F_z+(\bar{x}F_z+(\bar{x}F_x+\bar{y}F_y)\sqrt{m_\perp^*/m_\parallel^*}\,]\,. \quad (5)$$

Given the quadratic dependence on the electric field, the EA along the normal direction is expected to be $m_\parallel^*/m_\perp^*$ times larger than along the in-plane direction; i.e., $\Delta\alpha_\perp/\Delta\alpha_\parallel\approx m_\parallel^*/m_\perp^*$.

This change of coordinates allows us to use an effective isotropic Coulomb potential to replace the previous anisotropic one. For this purpose, we introduce the "isotropic" permittivity:

$$\varepsilon_{\text{eff}}\approx\tfrac{1}{3}[\varepsilon_z+(\varepsilon_x+\varepsilon_y)\sqrt{m_\perp^*/m_\parallel^*}\,]\,. \quad (6)$$

By applying the effective Coulomb potential in the new coordinate system, where the lowest-energy exciton observed corresponds to the hydrogenic $1s$ state of radius $a^*=\varepsilon_{\text{eff}}\hbar^2/m^*q^2$, the ratio of the line broadening to the Stark shift of the exciton energy E_{ex} is simply

$$\frac{\langle(\Delta E)^2\rangle}{\langle\Delta E\rangle}\approx\tfrac{8}{9}E_{\text{ex}}\,, \quad (7)$$

where

$$E_{\text{ex}}\approx-\frac{q^2}{2a^*\varepsilon_{\text{eff}}}\,. \quad (8)$$

Thus, if $\alpha(E)$ is known, measurement of the modulated absorption spectrum $\Delta\alpha(\mathbf{F})$ can be used to calculate the relative magnitudes of $\langle\Delta E\rangle$ and $\langle(\Delta E)^2\rangle$ via Eq. (3). This further allows for the estimation of the exciton binding energy, radius, and eccentricity, as well as the effective mass tensor.

For the in-plane electric-field measurement, electrodes were patterned directly onto a glass substrate precleaned by boiling in 1,1,1-trichloroethane, and successively rinsing in acetone and methanol. Metal layers consisting of 300 Å thick Ti followed by 1000 Å thick Au were electron-beam deposited and then photolithographically patterned to form a series of 5×100 μm^2 interdigitated electrodes with 5 μm spacings between adjacent fingers. For measurements where the electric field was applied normal to the substrate, a glass substrate precoated over 50% of its surface with indium tin oxide (ITO) was used to form the bottom electrode.

Substrates were loaded into a vacuum chamber (base pressure 10^{-7} Torr) and cooled to $\sim$90 K. For all samples, 1000 Å thick crystalline organic films of either PTCDA or PTCBI were grown by sublimation of the prepurified source material from a resistively heated, baffled molybdenum boat to achieve a growth rate of 3–5 Å/s ($\sim$1 monolayer/s) as measured using a quartz crystal thickness monitor. After film growth, a final 100 Å thick Au film was deposited from a tungsten boat onto the organic crystal surface through 0.1×1 cm^2 openings in a shadow mask to form the semitransparent top electrodes used in the normal-direction measurement.

To study EA due to a sinusoidally varying voltage (at frequency $f=840$ Hz and 30 kHz), unpolarized light from a monochromator was focused onto the electrode area. Light transmitted through the sample was collected and focused onto a silicon detector. The change in sample transmission due to the applied electric field was then measured with a lock-in amplifier. Since $\Delta\alpha$ is proportional to F^2, the lock-in was tuned to be sensitive at $2f$. Field-induced changes in the transmitted intensity ($\Delta I/I=-t\Delta\alpha$, where t is the sample thickness, and I is the intensity of the transmitted light) of 10^{-4} could be resolved by this means.

In Fig. 3, we plot the absorption and the EA spectra in the normal direction, $\Delta\alpha_\perp(\mathbf{F},\lambda)$, of the crystalline, 1000 Å thick PTCDA film (λ is the wavelength). Also shown is a fit of $\alpha(\lambda)$ to three exciton absorption lines with Gaussian profiles (dashed curve). The lowest-energy observed exciton peak of the bulk PTCDA absorption spectrum is at $\sim$555 nm, with higher-order exciton peaks at wavelengths <520 nm.[23] The film thickness for these measurements was chosen such that the signal for $\Delta\alpha$ was maximized near the absorption peak at 555 nm. Due to the high absorption coefficient and the reduced sensitivity of the silicon detector at $\lambda<500$ nm, very little transmitted light was detected at shorter wavelengths, giving rise to the large noise level. At $\lambda=560$ nm, we observe a maximum $\Delta\alpha=1000$ cm^{-1} at $F=600$ kV/cm. In addition, a peak at 505 nm is also observed, possibly corresponding to the Stark shift of higher-order excitons. However, due to the noise background in this wavelength range, the shape and the size of this peak are distorted. Since we are primarily interested in the EA corresponding to the lowest-energy observed exciton, we have not yet fully investigated the source of the higher-energy features.

In Fig. 4 we plot $\Delta\alpha$ vs F^2 at two different wavelengths and for both the normal and in-plane field directions. We observe a quadratic dependence of $\Delta\alpha$ on $\mathbf{F}$, as expected from Eq. (3), and also observe that at 565 nm the EA for in-plane fields $[\Delta\alpha_\parallel(\lambda)]$ is slightly smaller than $\Delta\alpha_\perp(\lambda)$. Figure 5 shows both $\Delta\alpha_\parallel(\lambda)$ and $\Delta\alpha_\perp(\lambda)$ (solid lines) in the normal and in-plane directions at $F\sim300$ kV/cm. We find that the shape and the magnitude of the curves are similar for the two field directions, where the small

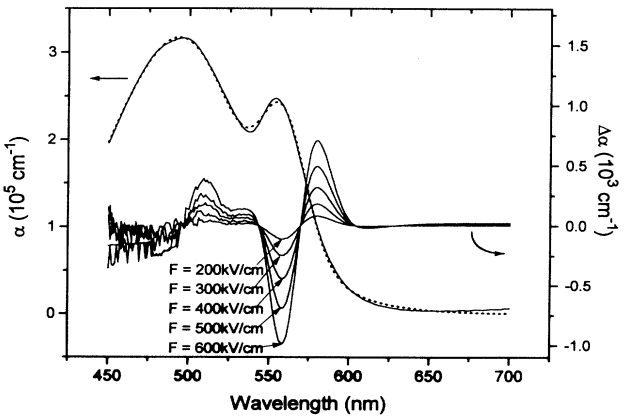

FIG. 3. Absorption and electroabsorption spectra of a 1000 Å PTCDA film. The dashed curve indicates a fit to the absorption using three Gaussian curves. The electroabsorption coefficient is plotted for electric fields ranging from 2×10^5 to 6×10^5 V/cm applied normal to the substrate plane.

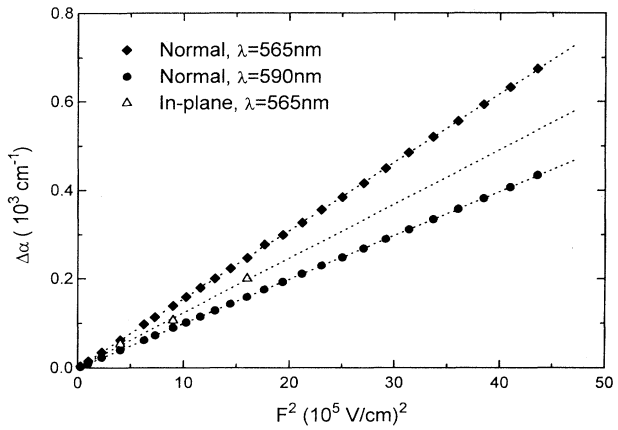

FIG. 4. Electroabsorption $\Delta\alpha$ as a function of squared applied electric field at two different wavelengths, with field applied in both the normal and in-plane directions.

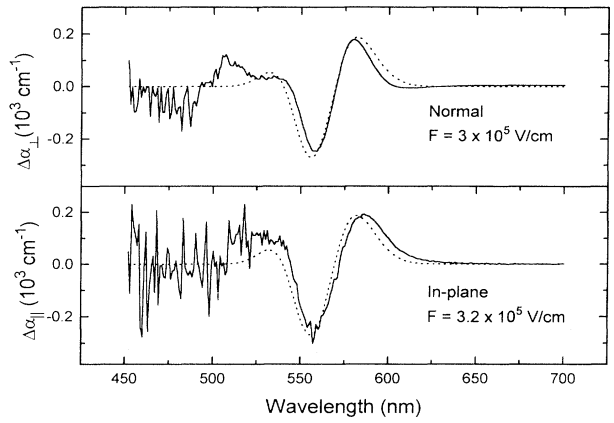

FIG. 5. Electroabsorption data (solid lines) and numerical fits (dashed lines) with fitting parameters listed in Table II. Top curve: field of 3×10^5 V/cm applied normal to the substrate plane. Bottom curve: field of 3.2×10^5 V/cm applied parallel to the substrate plane.

difference in magnitude is assigned to the anisotropic effective mass.

After extracting the lowest absorption peak from the fits to $\alpha(\lambda)$, we use the derivatives of this peak, and three parameters, $\langle(\Delta E)^2\rangle/\langle\Delta E\rangle$, $\langle\Delta E\rangle_\perp/\mathbf{F}_\perp^2$, and $\langle\Delta E\rangle_\parallel/\mathbf{F}_\parallel^2$, to fit the $\Delta\alpha(\mathbf{F},\lambda)$ curves. While $\langle(\Delta E)^2\rangle/\langle\Delta E\rangle$ expresses the relative size of broadening to the Stark shift, the latter two terms fit the Stark shift in the normal ($\perp$) and in-plane ($\parallel$) directions. The values of the parameters used to fit the data in Figs. 3 and 5 are given in Table II. The dashed curves in Fig. 5 are typical fits obtained using these parameters for measurements of $\Delta\alpha(\mathbf{F},\lambda)$ in both the normal and in-plane directions, and at fields ranging from 100 to 600 kV/cm. From these fits, the lowest observed exciton binding energy was found to be $-(150\pm15)$ meV, and the anisotropy of the effective hole mass was $m_\perp^*/m_\parallel^*\sim0.89\pm0.09$, which is surprisingly small given the anisotropic crystal structure.

In fitting these curves we also have to account for reflections from the several sample interfaces. That is, changes in $\Delta\alpha$ also lead to changes in Δn which change the transmittance of a lossy Fabry-Pérot cavity formed at the film interfaces via[24]

$$-\frac{\Delta I}{It}=\Delta\alpha+\frac{8\pi}{\lambda}\Delta n(\lambda)R\sin\delta e^{-\alpha t}\ . \tag{9}$$

Here, $R=\sqrt{R_1R_2}$ is the average reflectivity of the two interfaces, and $\delta=4\pi nt/\lambda$. Because the interface of PTCDA/air for in-plane measurements was less reflective ($R_1<3\%$) than the PTCDA/Au interface ($R_1\sim10\%$) used in the normal measurements, the Fabry-Pérot correction to $\Delta\alpha$ was larger for the normal measurement. This induces asymmetries in the measured EA along the two directions (shown "uncorrected" in Fig. 5). Using the PTCDA/glass/air interface reflectivity of $R_2\sim4\%$, then $R_\perp\sim5\%$ and $R_\parallel\sim2.5\%$ were used in fitting the curves in Fig. 5.

Using the dielectric tensor for PTCDA,[13] we calculate $\varepsilon_{\text{eff}}=3.46\pm0.35$ [see Eq. (6)]. From this value, the exciton radius along the normal direction is 14 ± 2 Å, and the in-plane radius is 13 ± 2 Å. The effective hole masses along the normal and in-plane directions can also be found by their relation to the exciton radius as $(0.13\pm0.02)m_0$ and $(0.14\pm0.03)m_0$, respectively, where m_0 is the free-electron mass (see Table III). These results are consistent with previous work which has shown that an average isotropic dielectric constant can be used to accurately calculate the exciton energy in a highly anisotropic crystal.[6]

The consistency between these values of the exciton mass and radius and those obtained previously by exciton confinement measurements,[9] as well as the success of using a simple set of hydrogenic wave functions together with an effective isotropic Coulomb potential to fit the EA spectra for PTCDA, suggest that the exciton can, in part, be described as a Wannier-like state. However, the

TABLE II. Parameters used to fit the PTCDA electroabsorption spectra.

Parameters	Symbol	Unit	Value
Broadening/Shift	$\langle(\Delta E)^2\rangle/\langle\Delta E\rangle$	$(\text{meV})^2/\mu\text{eV}$	0.17 ± 0.02
Energy shift/(field)^2 (normal direction)	$\langle\Delta E\rangle_\perp/\mathbf{F}_\perp^2$	$\mu\text{eV}/(10^5\text{ V/cm})^2$	11.1 ± 1.7
Energy shift/(field)^2 (in-plane direction)	$\langle\Delta E\rangle_\parallel/\mathbf{F}_\parallel^2$	$\mu\text{eV}/(10^5\text{ V/cm})^2$	9.9 ± 1.5

TABLE III. Summary of the PTCDA electroabsorption results.

Parameters	Symbol	Unit	Results from this work	Value from Ref. 9
Exciton binding energy	E_{ex}	meV	-150 ± 18	
Exciton radius along normal direction	$a_{\perp}^{*}$	Å	13.8 ± 2.0	12 ± 1
Exciton radius along in-plane direction	$a_{\parallel}^{*}$	Å	13.0 ± 2.0	12 ± 1
Effective hole mass along normal direction	$m_{\perp}^{*}$	m_0	0.13 ± 0.02	0.18 ± 0.01
Effective hole mass along in-plane direction	$m_{\parallel}^{*}$	m_0	0.14 ± 0.03	

CT nature of the exciton is also important for fully describing the broadening observed in the EA spectrum. This surprising degree of Wannier content of the PTCDA exciton is a result of the extremely close packing of the molecules, which leads to a high degree of π-orbital overlap in the normal direction.

Similar measurements were performed on 1000 Å thick layers of PTCBI deposited on substrates similar to those used for PTCDA. Electric fields were applied in both the normal and in-plane direction using fields of similar magnitude to those used for PTCDA. Under these conditions, no change in PTCBI absorption was observed as a function of applied electric field. Given our measurement sensitivity, we can set a limit of $\Delta\alpha \leq 60$ cm^{-1} at $F \sim 600$ kV/cm for PTCBI. From this, an exciton binding energy of >700 meV is inferred, corresponding to a radius of $a^* \leq 3$ Å. Thus, excitons in PTCBI do not exhibit a significant CT component due to their smaller radius; i.e., PTCBI excitons are Frenkel-like. This conclusion is corroborated by absorption and fluorescence data to be discussed in Sec. IV. The structural differences between PTCDA and PTCBI which lead to their different spectral properties have been considered in Sec. II, and will be discussed further in Sec. V.

IV. EXCITONS IN CONFINED STRUCTURES

In a second series of experiments, we measured low-temperature absorption and fluorescence spectra to determine the effects of restricting excitons in ultrathin layers of thickness t, where t is on the order of the exciton radius, a^*. For these experiments, alternating multilayer stacks of PTCDA and NTCDA, or PTCBI and NTCDA layers, were grown on glass substrates maintained at ≈ 90 K during growth.[8] Growth was accomplished by sublimation of the organic compounds at a rate of 0.1–0.3 Å/s from a Knudsen effusion cell in an ultrahigh-vacuum OMBD chamber with a base pressure of $<5\times10^{-11}$ Torr. Growth rates and layer thicknesses were measured using a quartz crystal thickness monitor placed near the substrate. Sequential shuttering of the effusion cells was used to grow alternating layers of both PTCDA/NTCDA and PTCBI/NTCDA until the total thickness of all of the PTCDA or PTCBI layers was 500–600 Å. The thickness of the intermediate NTCDA layers matched the PTCDA or PTCBI layer thicknesses, except for the 50-period 10 ± 5 Å PTCDA structures. In this case, the NTCDA thickness was increased to 20 Å to ensure growth of a continuous layer due to the larger interplanar stacking distance and tilt angle in the NTCDA structure (see Table I and Fig. 1).

NTCDA was used as the intermediate layer since its lowest-energy exciton state is ~1 eV greater than the excited-state energies in PTCDA and PTCBI. These multilayer structures are therefore similar to inorganic semiconductor multiple-quantum-well structures, where the quantum-well material is either PTCDA or PTCBI and the "larger-band-gap" or barrier material is NTCDA.

For all of the spectral measurements, samples were immersed in liquid helium to narrow the broad spectral features which are due to the strong exciton-phonon coupling in these organic compounds. For measurements of absorption spectra, a white light was focused onto the sample surface and the transmitted light was analyzed with a monochromator. For measurements of fluorescence spectra, samples were optically excited with the 488 nm line of an Ar^+ ion laser with an intensity of <500 W/cm^2. Upon illumination at this wavelength, excitons were generated predominantly in the PTCDA or PTCBI layers in the multilayer stacks. Fluorescence was then collected from the front surface of the sample and detected with either a photomultiplier tube or a silicon photodiode array after passing through a monochromator.

A. PTCDA/NTCDA multilayer stacks

Low-temperature (4.2 K) fluorescence spectra of multilayer stacks of alternating layers of PTCDA and NTCDA, where PTCDA layer thicknesses were varied from a single "bulk" thin film of 500 Å to a structure consisting of a 50-period stack of 10 ± 5 Å PTCDA films (~3 monolayers) separated by NTCDA, are shown in Fig. 6. Four equally spaced peaks labeled A, B, C, and D are observed, indicative of vibronic transitions from the excited to the ground state. Note that not all of the peaks A through D are present in all of the spectra. The energy spacings ω_{ph} of the vibronic peaks are observed to increase from 1065 cm^{-1} at 500 Å to 1226 cm^{-1} for the thinnest, 10 Å layers. The change in ω_{ph} (or $\Delta\omega_{ph}$) in PTCDA films as a function of layer thickness, as refer-

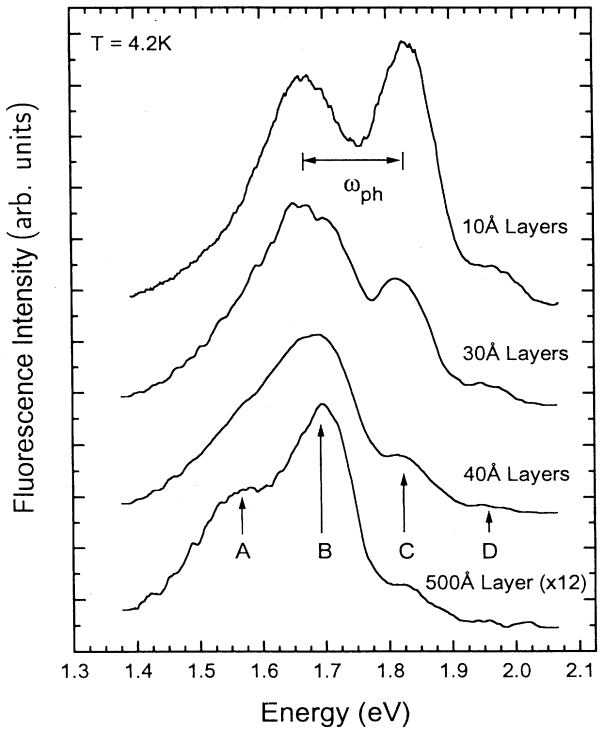

FIG. 6. Low-temperature (4.2 K) fluorescence spectra of PTCDA/NTCDA multilayer stacks for layer thicknesses of PTCDA ranging from 10 to 500 Å. The four peaks in the spectra are labeled *A*, *B*, *C*, and *D*, and the spectra are displaced vertically for clarity.

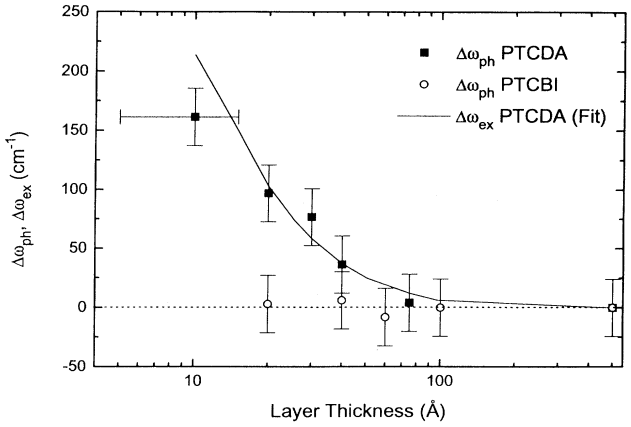

FIG. 7. Measured change in the ground-state vibrational frequency, $\Delta\omega_{ph}$, of both PTCDA (squares) and PTCBI (open circles) as a function of layer thickness, as referenced to their respective 500 Å films. The solid line is a fit to data of the observed exciton energy shift ($\Delta\omega_{ex}$) in PTCDA layers using the theory in Ref. 9.

enced to the 500 Å film is shown by the solid squares in Fig. 7. For each measurement, $\Delta\omega_{ph}$ is found by fitting the appropriate fluorescence spectrum to a series of four overlapping Gaussian curves. This procedure yields both the peak position and width, where we have found that the full width at half maximum (FWHM) of the fluorescence peak at ~ 1.67 eV, for example, increases from 216 to 330 meV as the layer thickness is decreased from 500 to 10 Å. This broadening has previously been attributed to interface roughness in organic multilayer systems.[25]

The change in vibrational frequency, $\Delta\omega_{ph}$, as a function of layer thickness is accompanied by an increase in the fluorescence intensity of the high-energy transitions at the expense of the low-energy transitions. This progressive redistribution of fluorescence intensity through the four separate fluorescence peaks in PTCDA was only observed at 4.2 K, while at higher temperatures the separate lines broaden and merge into a single feature whose peak shifts to higher energy as layer thickness is decreased.[26] A plot of the fluorescence of the 10 Å PTCDA multilayer stack as a function of pump intensity is shown in Fig. 8. In the inset, a plot of the intensity of each of the three peaks is shown to be linear with pump intensity. Since both the spectral shape and the fluorescence efficiency remain constant with pump intensity, we conclude that the conditions used are far from those leading to band filling or other nonlinear effects. In addition, we observe that the fluorescence intensity of the 10 Å film is approximately 12 times larger than for the 500 Å PTCDA film. This indicates that interfaces assist in the radiative recombination of excitons in PTCDA layers, as well as suggesting that a very low density of interfacial defects, which would be expected to lead to fluorescence quenching, exists at the PTCDA/NTCDA heterointerface. Indeed, this increased radiative recombination is characteristic of exciton spatial confinement due to an increased overlap of the electron and hole wave functions.[27]

A comparison of the low-temperature (4.2 K) absorbance spectra of a single 500 Å thick PTCDA layer and a 50-period stack of 10±5 Å PTCDA/20 Å NTCDA is shown in Fig. 9. A graph of the derivative of the absorption with respect to photon energy, $(d\alpha/dE)$, in the energy range of the lowest-energy observed exciton peak is shown in the inset of Fig. 9. Note that the peak at 2.234 eV is shifted to higher energy (as shown clearly in the zero crossing of each derivative curve) as the layer thickness is decreased. Previously,[9] this shift was attributed to the change in the exciton binding energy as a result of quantum confinement in a finite potential well. The potential-well width corresponded to the PTCDA layer thickness, and it was suggested that the energy barriers were provided by the HOMO offsets at the heterointerfaces with NTCDA layers. In that work, the Schrödinger equation for the system was solved by minimizing the exciton binding energy as a function of radius, and fitting the theoretical result to the absorption spectral peak shifts and fluorescence decay times. The best fit, shown as the solid line in Fig. 7, assumes that the radius of the lowest-energy observed exciton in PTCDA is ~ 12 Å, or 3–4 molecules in the stacks of PTCDA normal to the substrate. This is in agreement with the determination of the exciton radius from the EA spectra in Sec. III (see Table III).

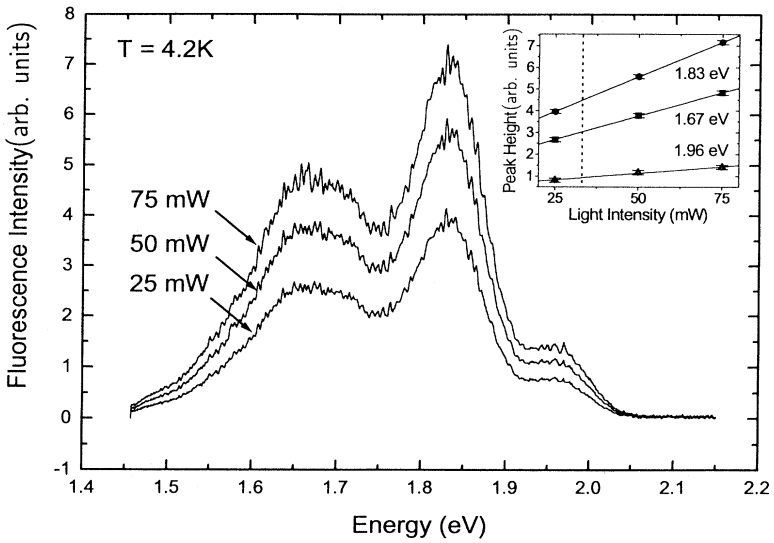

FIG. 8. Low-temperature (4.2 K) fluorescence spectra of a 10 Å PTCDA/NTCDA multilayer stack as a function of 488 nm Ar^+ laser pump intensity. Inset: Heights of the individual fluorescence peaks of the 10 Å PTCDA/NTCDA multilayer stack as a function of pump intensity. The vertical dashed line indicates the pump intensity used to obtain the spectra in Fig. 6.

Note that the blueshift of the exciton absorption peak in PTCDA in Fig. 7 matches the increase in the vibrational frequency of the molecular ground state. This suggests that the exciton blueshift observed in absorption, and the increase in ground-state vibrational frequency observed in fluorescence, are related through strong exciton-phonon coupling. This conclusion is supported by the very large Franck-Condon energy observed in PTCDA,[28] and will be analyzed quantitatively in Sec. VI.

B. PTCBI/NTCDA multilayer stacks

Low-temperature fluorescence spectra of multilayer stacks of PTCBI layers alternated with NTCDA layers, where PTCBI layer thicknesses were varied from 20 to 500 Å, are shown in Fig. 10. Note that two peaks in the spectra are clearly resolved at 1.478 and 1.427 eV. As the PTCBI layer thickness is decreased to a 25-period stack of 20 Å PTCBI alternated with 20 Å NTCDA, the only change observed in the fluorescence spectrum is a small but significant redistribution of fluorescence intensity to higher energy, and a peak width broadening previously attributed to interface roughness.[25] The change in spacing between the two peaks in the PTCBI fluorescence spectra as a function of layer thickness is shown by the open circles in Fig. 7. Assuming that the peaks are due to the same dominant vibration, then Fig. 7 indicates that the vibrational frequency in PTCBI does not change significantly as layer thickness is decreased ($\Delta\omega_{ph} \sim 0$), in contrast to the clearly observed frequency changes in PTCDA.

As was observed in PTCDA multilayer stacks (Fig. 8), both the spectral shape and fluorescence efficiency of PTCBI films remain constant for the range of optical pump intensities used in the experiment. In addition, the fluorescence efficiency of PTCBI was found to increase by only a factor of 3 from the widest (500 Å) to the narrowest (20 Å) layers. This is in contrast to the twelvefold increase in PTCDA fluorescence efficiency as layer thickness was reduced over a similar range. This indicates

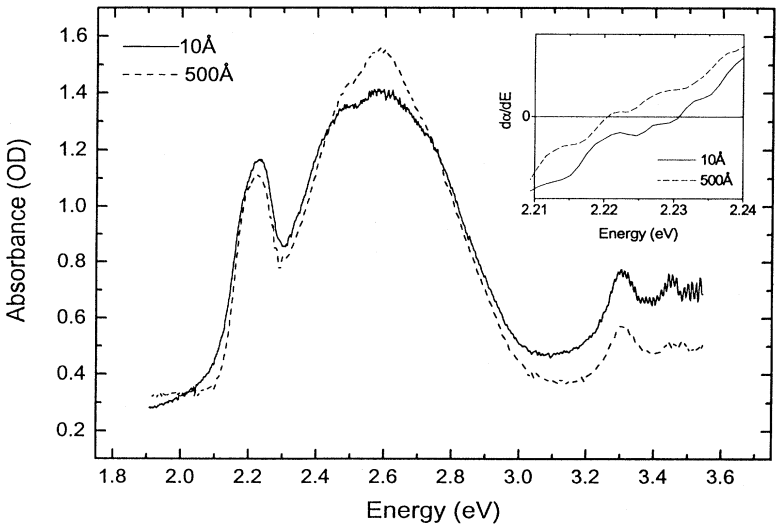

FIG. 9. Low-temperature (4.2 K) absorption spectra of a 500 Å PTCDA film and a 10±5 Å PTCDA/20 Å NTCDA multilayer stack. Inset: Change in absorption coefficient as a function of energy, $d\alpha/dE$, for the samples in Fig. 9.

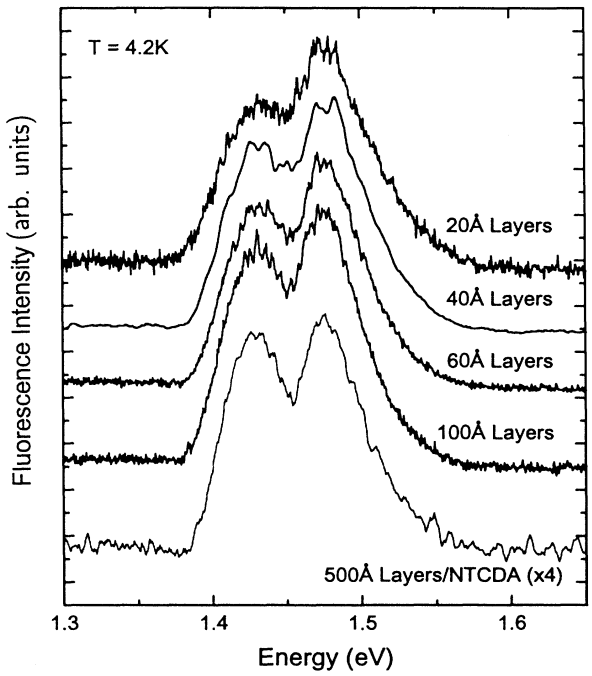

FIG. 10. Low-temperature (4.2 K) fluorescence spectra of PTCBI/NTCDA multilayer stacks for layer thicknesses of PTCBI ranging from 20 to 500 Å. The spectra are vertically displaced for clarity.

that neither the presence of heterointerfaces nor exciton confinement in the PTCBI multilayer stacks are as active in enhancing radiative recombination as they are in the PTCDA multilayer stacks.

Figure 11 shows a comparison of the low-temperature absorbance spectra of a five-period 100 Å PTCBI stack and a 25-period 20 Å PTCBI stack. Note that no peak shifts between the two spectra are observed, in contrast to the exciton blueshift with decreasing PTCDA layer thicknesses apparent in Fig. 9. This result is consistent with the EA measurements for PTCBI, where a small-radius ($a^* \leq 3$ Å) exciton is observed which is unlikely to exhibit confinement effects for the range of layer thicknesses used in these experiments.

V. ANALYSIS OF EXCITONS IN CONFINED STRUCTURES

To quantitatively understand the spectral dependence on layer thickness, we assume an adiabatic system where a single totally symmetric vibrational mode is dominant in the ground state. In addition, the ground state is assumed to be parabolic, accounting for the single value of ω_{ph} between the PTCDA vibronic transitions *A*, *B*, *C*, and *D* in Fig. 6. Figure 12 shows the molecular potential-energy diagrams of both a thin [Fig. 12(a)] and a thick [Fig. 12(b)] PTCDA layer, indicating the optical transitions between the excited and ground states. In this diagram, the electronic energy levels are plotted with respect to the molecular configurational coordinate q_m. The horizontal lines in the potential curves denote the energy of the dominant intramolecular vibrational mode. As noted earlier, the excitonic wave functions depicted in Fig. 12 can extend over several molecules.

The transition dipole moment of a vibronic transition is proportional to the electronic transition dipole moment multiplied by the overlap integral of the vibrational wave functions in the excited and ground states. As shown in Fig. 6, since the fluorescence intensity continuously shifts to higher energy while maintaining an approximately constant total intensity over the range of layer thicknesses from 10 to 100 Å, we conclude that the observed vibronic transitions in PTCDA occur between the same excited- and ground-state manifolds. The observed transitions, therefore, have the same electronic transition dipole moment, and the changes in the fluorescence spectra are simply due to changes in the vibrational wave function overlap with layer thickness. Now, assume that all vibronic transitions occur after the system reaches thermal equilibrium at the lowest level in the excited state (0′). This assumption is supported by relaxation-time measurements of molecular vibrations of 0.2 ps,[29] as

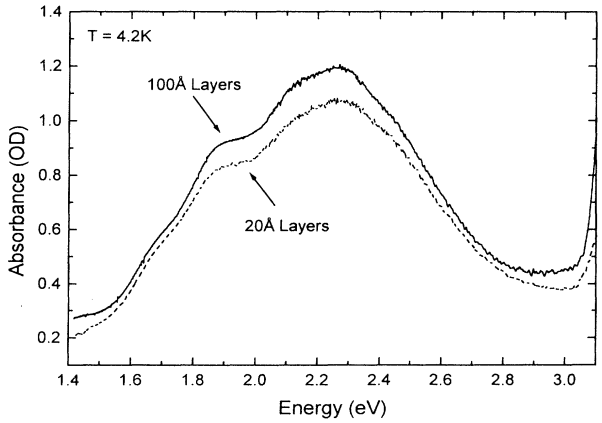

FIG. 11. Low-temperature (4.2 K) absorption spectra of a 100 Å PTCBI/NTCDA multilayer stack and a 20 Å PTCBI/NTCDA multilayer stack.

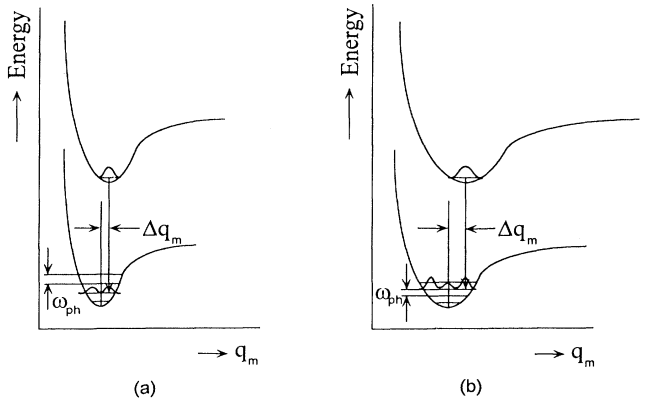

FIG. 12. Configurational coordinate diagram showing the relative changes in the excited- and ground-state molecular potential-energy wells of (a) thin and (b) thick PTCDA films.

compared to the exciton lifetime of ~ 10 ns.[2,8] In this case, the change in vibrational frequency, $\Delta\omega_{ph}$, for PTCDA (Fig. 7) is due to an increase in the molecular force constant (k), or curvature, of the molecular potential-energy well as layer thickness decreases (Fig. 12), via $\Delta k = 2m_r\omega_{ph}\Delta\omega_{ph}$, where m_r is the reduced mass of the vibrating intramolecular C-C bond.

To account for the observed redistribution of intensity to higher-energy vibronic transitions, a change in the relative equilibrium configurational coordinate of the excited (q_m') and ground states (q_m^0) is assumed, where $\Delta q_m = q_m' - q_m^0$ decreases with layer thickness (Fig. 12). In the Condon approximation, the oscillator strengths of the transitions from the lowest vibrational level of the upper (excited) manifold ($u0$) to the nth excited vibrational level of the lower (ground) manifold ($1n$) can be described by a Poisson distribution,[30,31] viz.

$$f_{u0,1n}(x) \cong f_{u1}\frac{x^n}{n!}e^{-x}, \tag{10}$$

where

$$x = \frac{1}{2}\frac{k(\Delta q_m)^2}{\hbar\omega_{ph}}, \tag{11}$$

f_{u1} is the sum of the oscillator strengths of the vibronic transitions, and n is the vibrational level index in the ground state which ranges from 0 (lowest energy) to 3 (third excited vibrational level) for the four observed spectral peaks. If we measure the ratio of the intensities of the vibronic transitions in Fig. 6 employing the same Gaussian peak fitting procedure used to obtain ω_{ph}, we can fit Eq. (10) to the observed vibrational progressions as a function of Δq_m. A calculation of $f_{u0,1n}(x)/f_{u1}$ for $n = 0-3$ is shown by the solid curves in Fig. 13, where the measured ratios of the peak heights of each of the individual vibronic transitions in the sample spectra are shown by the data points. For the vibrational progression of fluorescence peaks labeled A,B,C,D in Fig. 6 to fit Eq. (11), the relative intensities of the individual vibronic peaks for each layer thickness must lie on a single vertical line; i.e., each multilayer stack must be characterized by a single value of x. Hence the data points for each sample must lie at the intersections between the dashed vertical lines and the solid curves. We note that the excellent fits obtained for all layer thicknesses show that the structure observed in the fluorescence spectra is indeed due to discrete vibronic transitions which occur upon recombination of the multimolecular excitons present in PTCDA, and that the narrowing and equilibrium coordinate displacement of the molecular potential-energy wells (Fig. 12) are largely unaffected by structural defects introduced during growth, since these effects would tend to result in significant deviations from the simple form given by Eq. (10).

Using the values obtained for x and Eq. (11), Δq_m vs layer thickness is plotted in Fig. 14. For this calculation, we assume $m_r = 6$ amu, consistent with a C-C bond vibration. Here, Δq_m is found to continuously *decrease* with PTCDA layer thickness over the range of 500 to 10 Å. The magnitude of Δq_m corresponds to a large molecular

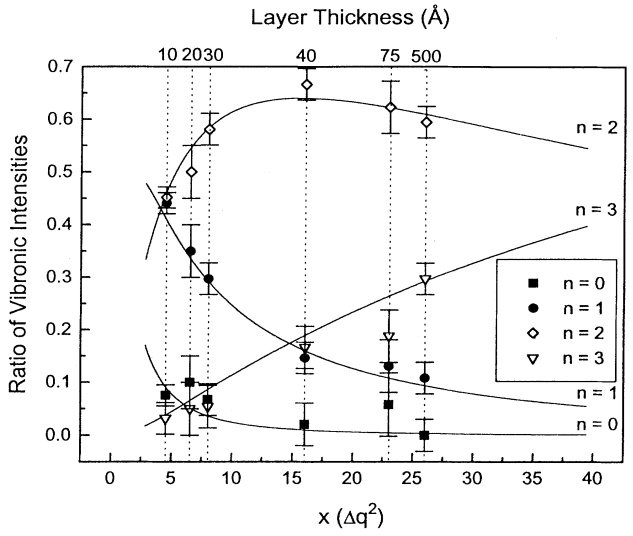

FIG. 13. Relative strengths of the individual vibronic level transitions $f_{u0,1n}/f_{u1}$ in PTCDA are shown by the solid curves for values of n (vibrational level index) ranging from 0 to 3. The peaks labeled A,B,C,D in Fig. 6 correspond to the four values of n. Data obtained from the measured fluorescence spectra for PTCDA samples ranging in layer thickness from 10 to 500 Å are shown as points. Vertical lines correspond to the values of x resulting from best fits to the data for each sample layer thickness.

conformational change upon excitation which must take place in PTCDA with its exceptionally large Franck-Condon energy (Fig. 15), broad absorption spectrum, and lack of mirror symmetry between fluorescence and absorption.[32]

Since Δq_m corresponds to the *total* molecular conformational change upon excitation, our results suggest that

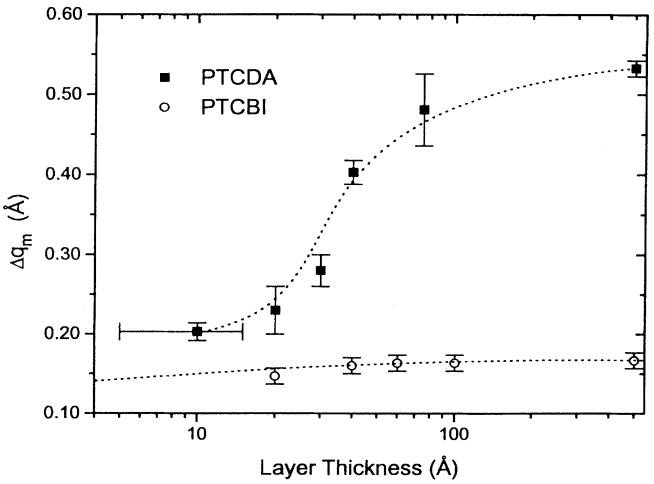

FIG. 14. Change in the relative equilibrium configurational coordinate (Δq_m) of the excited and ground states as a function of layer thickness for both PTCDA and PTCBI films. Lines are drawn as a guide to the eye.

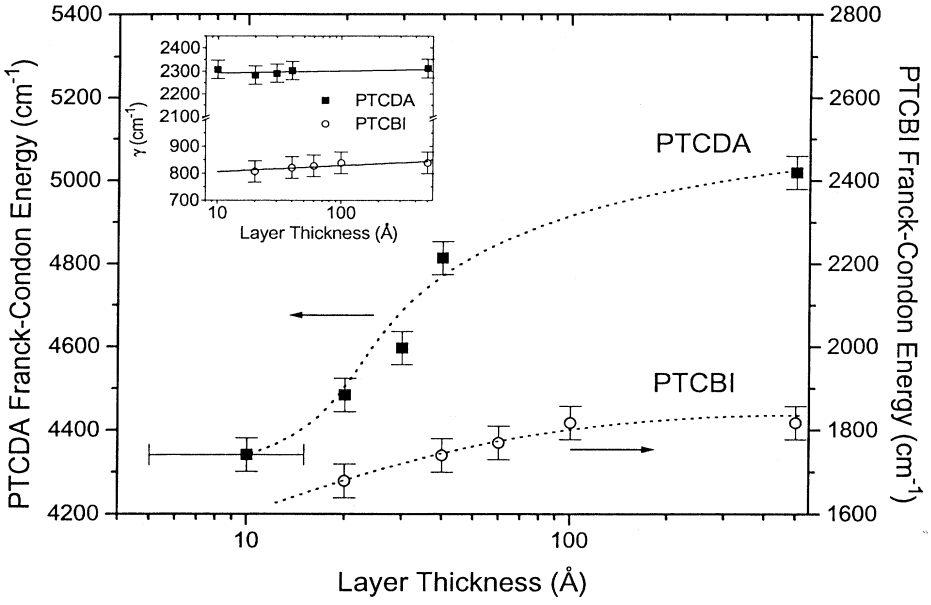

FIG. 15. Franck-Condon energy in PTCDA and PTCBI, measured as the difference from the 0-0 absorption peak to the first moment (see Ref. 34) of the fluorescence spectrum. Lines are drawn as a guide to the eye. Inset: Exciton-phonon coupling frequency γ as a function of layer thickness for both PTCDA and PTCBI.

the decrease in Δq_m with layer thickness is due to exciton confinement in ultrathin layers. That is, as the layer thickness is decreased, the exciton overlaps with fewer molecules,[9] so that the total conformational change of the excited molecules is reduced. Similarly, a reduced exciton radius in the ultrathin layers[9] will result in a decreased dipole moment, which in turn will cause a decreased conformational change. This is consistent with previous studies of the absorption spectra of organic/inorganic multilayer stacks, where it was suggested that the intermolecular interaction decreases with layer thickness.[33]

The molecular potential-energy-well diagrams shown in Fig. 12 may also be used to understand PTCBI/NTCDA multilayer stacks. Since little or no change in vibrational frequency $\omega_{\rm ph}$ is observed in those structures (Fig. 7), we infer that there is an insignificant change in the curvature of the potential-energy wells with decreasing layer thickness. To account for the small redistribution of fluorescence intensity between the peaks in the fluorescence spectra, we can calculate Δq_m for PTCBI following the above procedure by assuming that the spacing between the two fluorescence peaks determines the dominant vibrational frequency, and that the peaks correspond to the highest-energy and next-highest-energy vibronic transitions. With these assumptions, $\Delta q_m \approx 0.17$ Å. This value for Δq_m in PTCBI, also shown in Fig. 14, is roughly one-third that of PTCDA, and shows only a minimal dependence on layer thickness over the range used in these measurements.

Figure 15 is a plot of the Franck-Condon energy ($E_{\rm FC}$) in both PTCDA and PTCBI as a function of layer thickness. Here, $E_{\rm FC}$ is measured from the lowest-energy absorption peak to the first moment[34] of the fluorescence spectrum. Since $E_{\rm FC}$ can be defined as[28,30]

$$E_{\rm FC}=\frac{\hbar\gamma^2}{\omega_{\rm ph}}\ , \tag{12}$$

where γ is the exciton-phonon coupling frequency, then using the values measured for $E_{\rm FC}$ (Fig. 15) and $\omega_{\rm ph}$ (Fig. 7) we calculate γ for PTCDA and PTCBI, shown in the inset of Fig. 15. The exciton-phonon coupling is found to be independent of layer thickness. This result is expected for layers whose *structure* is independent of layer thickness, which is indeed found to be the case for PTCDA and PTCBI layers grown by OMBD using the conditions described in Secs. II and IV. Finally, we observe that γ in PTCBI is roughly one-third that of PTCDA, consistent with the difference in Δq_m between these materials (Fig. 14), and showing that $\gamma \propto \Delta q_m$, as expected.[30] All of these results indicate an internal consistency between measurements of $E_{\rm FC}$, γ, Δq_m, and $\omega_{\rm ph}$, suggesting that the spectral differences between PTCDA and PTCBI are *intrinsic* rather than being due to interface effects or disorder in the thin films.

VI. DISCUSSION

The analyses of the electroabsorption and the spectral dependences on layer thickness have shown that spatially extended CT excitons exist in PTCDA while Frenkel excitons dominate the spectral features in PTCBI. In addition, analysis of the fluorescence spectra has shown that the amount of molecular conformational change upon excitation decreases with layer thickness in ultrathin layers of PTCDA. We note that intermolecular CT excitons couple strongly to the phonon system, since there is a considerable change in the dipole moment which accompanies the creation of an excited state.[35] Therefore, to quantitatively investigate the exciton-phonon interactions in strongly coupled OMC's such as PTCDA, and in particular to understand why the absorption blueshift ($\Delta\omega_{\rm ex}$) and change in phonon frequency ($\Delta\omega_{\rm ph}$) with layer thickness are similar in magnitude (Fig. 7), we consider the Hamiltonian which describes the interaction of excitons and phonons with external radiation fields. Assuming the

rotating-wave approximation while keeping only the linear exciton-phonon interaction without any phonon-phonon interactions, the Hamiltonian is

$$H=\hbar(\omega_{ex}-\omega)a^{\dagger}a+\sum_{\beta}\hbar\omega_{ph,\beta}b_{\beta}^{\dagger}b_{\beta}$$
$$-\sum_{\beta}\hbar\gamma a^{\dagger}a(b_{\beta}+b_{\beta}^{\dagger})-\tfrac{1}{2}\mu a^{\dagger}F-\tfrac{1}{2}\mu aF^{*}\ , \quad (13)$$

where $\hbar\omega_{ex}$ is the exciton binding energy, ω is the photon frequency, $\hbar\omega_{ph,\beta}$ is the phonon energy of phonon mode index β, and μ is the electric dipole moment of the exciton. Further, $a^{\dagger}(a)$ and $b_{\beta}^{\dagger}(b_{\beta})$ are the exciton and phonon creation (annihilation) operators, respectively.

Following the treatment of Lam, Forrest, and Tangonan,[28] the exciton population ($a^{\dagger}a$) and phonon amplitude ($b_{\beta}+b_{\beta}^{\dagger}$) are calculated from the Heisenberg equation of motion. In steady state, assuming the external field F is small and only a single dominant phonon mode is present, we obtain the relationships

$$a^{\dagger}a\cong\frac{\Omega^{2}}{\eta^{2}+\delta^{2}} \quad (14)$$

and

$$b+b^{\dagger}=\frac{2\gamma a^{\dagger}a}{\omega_{ph}}\ . \quad (15)$$

In Eq. (14), $\Omega=\mu F/2\hbar$ is the Rabi frequency, δ is the exciton dephasing rate, and $\eta=(\omega_{ex}-\omega)$ is the detuning from the exciton resonance. In general, δ is much smaller than the exciton frequency ω_{ex}. Recognizing that the second summation in Eq. (13) is the exciton-phonon interaction, then from Eqs. (14) and (15) we obtain for the exciton-phonon interaction energy

$$E_{int}=-2E_{FC}\left[\frac{\Omega}{\eta}\right]^{4}\ . \quad (16)$$

From Eq. (16), assuming that E_{int} is independent of changes in E_{FC} or E_{ex} which accompany a reduction in layer thickness, and using $\Delta\eta=\Delta\omega_{ex}$, it is apparent that

$$\frac{\Delta E_{FC}}{E_{FC}}=4\frac{\Delta E_{ex}}{E_{ex}}=-\frac{\Delta\omega_{ph}}{\omega_{ph}}\ . \quad (17)$$

Thus the change in the exciton binding energy ($\Delta E_{ex}=\hbar\Delta\omega_{ex}$) is *directly proportional to the change in the phonon frequency* ($\Delta\omega_{ph}$) with layer thickness. For our samples, we find that $\Delta\omega_{ph}$ (and thus ΔE_{FC}) is approximately one-fourth of the value predicted by this simple expression (solid line, Fig. 7). This difference may be due to an increase in E_{int} with layer thickness which was not considered in the derivation of Eq. (17). Here, E_{int} corresponds to the polaron energy, where the presence of an exciton causes a local distortion of the lattice.[1,36] The decreasing polaron energy with decreased layer thickness suggests that the exciton in the ultrathin layer induces a smaller distortion in the lattice. Indeed, since $E_{int}\propto\mu^{4}$ [cf. Eq. (16)], the data in Fig. 7 suggest that the dipole moment decreases by approximately 10% as the layer thickness is decreased from 500 to 10 Å. Since μ is proportional to the exciton radius a^{*}, we conclude that a^{*} is also decreased by a similar amount in the thinnest layers. This reduction in exciton radius is a consequence of confinement of extended exciton states, and is consistent with previous calculations of excitons in crystalline organic thin films,[9] as well as with the observed molecular conformational changes shown in Fig. 14.

From results for PTCDA/NTCDA multilayers, we conclude that the effects of confinement are significant due to the relatively large spatial extent of the exciton. These results are in contrast to those for PTCBI/NTCDA, where the PTCBI exciton is largely unaffected by the ultrathin layers, due to its small-radius, Frenkel-like nature. To explain these differences between PTCDA and PTCBI, we propose three possibilities. (i) Since the imidazole group in the preferentially hole-transporting PTCBI (Ref. 37) acts as an electron donor, we speculate that holes are easily trapped on the excited molecules, leading to the formation of Frenkel excitons. (ii) The random distribution of the two isomers present in the PTCBI crystal might lead to a disruption of the π-orbital overlap between adjacent molecules in a stack, thereby limiting the spatial extent of the exciton. (iii) Calculation of the electronic overlap of the p orbitals of adjacent carbon atoms in two different molecules indicates that the overlap is over three times greater at a PTCDA-PTCDA molecule spacing of 3.21 Å compared to the PTCBI-PTCBI molecule spacing of 3.45 Å. This implies that intermolecular carrier transfer is significantly reduced in PTCBI due to its relatively large interplanar stacking distance.

The very weak spectral dependences on layer thickness observed in PTCBI/NTCDA may alternatively be explained by the absence of confining activation energy barriers at the heterointerfaces between PTCBI and NTCDA. However, the HOMO offset at the PTCBI/NTCDA heterointerface exceeds that of the PTCDA/NTCDA stack by $\sim$0.2 eV.[37] This large activation energy barrier for PTCBI/NTCDA would be expected to lead to significant exciton confinement when $t\sim a^{*}$. We conclude, therefore, that the small-radius PTCBI exciton is not confined in the "thick" layers used in these experiments, and thus no spectral changes are observed.

In exploring the functional dependence of spectral characteristics on layer thickness in both PTCDA and PTCBI, we are able to eliminate previous questions about sources of the observed spectral changes. As discussed in previous work,[38,39] the lowest electronic excitation of molecules at a film surface often shows a blueshift in emission as compared to the bulk. Therefore, molecular excitons at *interfaces* in multilayer stacks can potentially be shifted in energy from their bulk values, in a similar but perhaps less pronounced fashion. Based on this assumption, the blueshift of the lowest-energy observed exciton in PTCDA with layer thickness may alternatively be explained as being due to a "small-radius" (Frenkel) exciton trapped at the PTCDA/NTCDA interface. However, no blueshift is observed for identically grown

analogous structures of PTCBI/NTCDA (Figs. 10 and 11). Now, the energy shift of the surface exciton is attributed to the difference in polarizability between the two contacting materials; e.g., PTCDA and NTCDA, or PTCBI and NTCDA. However, we anticipate a *larger* polarizability difference at the PTCBI/NTCDA heterointerface, as inferred from the large HOMO band-offset energies[37] referred to above. Furthermore, EA measurements indicate that the PTCDA exciton has $a^* \sim t$, whereas for PTCBI $a^* \ll t$. Therefore we conclude that the effects observed in the PTCDA/NTCDA multilayer stacks are a consequence of this large PTCDA exciton radius, rather than of exciton trapping at the interfaces.

An alternative explanation of these spectral variations with layer thickness is that interfacial disorder might lead to the observed blueshifts and changes in fluorescence. However, we have demonstrated that the growth of both PTCDA and PTCBI results in ordered crystalline layers, and therefore infer that the relatively small amount of interfacial disorder in multilayer stacks formed with these two analogous molecules and NTCDA is comparable. Therefore the differences in the spectral changes for PTCDA and PTCBI are not likely to be due to disorder, consistent with our result that γ is independent of layer thickness (Fig. 15).

VII. CONCLUSIONS

From the analysis of the electroabsorption of crystalline organic thin films grown by the ultrahigh-vacuum process of organic molecular-beam deposition, we determine the radii of the lowest-energy observed excitons in bulk films of two organic molecular crystals. In PTCDA, a nearly spatially symmetric charge-transfer/Wannier-like exciton with a radius of ~ 13 Å is observed. In PTCBI, a much smaller CT component to the exciton is observed, suggesting that the exciton in this analogous molecule to PTCDA has a radius of ≤ 3 Å, i.e., it is a Frenkel state.

The fluorescence and absorption spectra of multilayer stacks of ultrathin layers of both PTCDA and PTCBI have been presented. In PTCDA/NTCDA multilayer stacks, we observe an increase in the vibrational energies of the ground state, as well as a redistribution of fluorescence intensity from lower- to higher-energy vibronic transitions as the layer thickness is decreased from 500 to 10 Å. In contrast, no change in the vibrational energies of the ground state is observed in PTCBI/NTCDA structures, and only a small redistribution of fluorescence intensity to higher-energy transitions is found as layer thickness is decreased. From these observations, we find that spatially extended CT excitons exhibit confinement effects in ultrathin PTCDA layers, but excitons in PTCBI do not display similar effects due to their smaller radius.

Exciton confinement in PTCDA leads to a shift in the relative equilibrium configurational coordinates of the excited and ground states. This indicates that confinement in ultrathin layers causes a reduced molecular conformational change upon excitation. In PTCBI, however, since the tightly bound Frenkel exciton shows relatively little dependence on layer thickness, only a small change in the shape of the molecule upon excitation is observed as a function of layer thickness. These differences have been attributed to differences in the crystalline and compositional structures of these two archetype OMC's.

Finally, a theoretical analysis of the interaction of excitons and phonons in organic molecular crystals with strong exciton-phonon coupling predicts that the exciton and phonon energies scale similarly when layer thickness is decreased in multilayer stacks. The predicted relations are confirmed by experimental results.

The analyses of absorption, fluorescence, and electroabsorption spectra, as well as the Franck-Condon energy, exciton-phonon coupling, and film composition, are all consistent with a model of exciton confinement in highly ordered crystalline organic thin films. Effects such as the trapping of excitons at surfaces and crystalline disorder are ruled out as explanations of the several observed spectral dependences on layer thickness.

ACKNOWLEDGMENTS

The authors thank Dr. J. F. Lam for enlightening discussions on the nature of exciton-phonon interactions, and Dr. L. S. Sapochak for discussions about the chemical differences between PTCDA and PTCBI. We thank D. Ho for the x-ray analysis of PTCBI. The authors thank the Air Force Office of Scientific Research (G. Pomrenke and C. Lee) and ARPA (A. Husain) for their generous support of this research. One of the authors (E.I.H.) thanks Rockwell International for support provided through the University of Southern California.

---

*On leave from the Department of Electrical Engineering/Electrophysics, University of Southern California, Los Angeles, CA 90089.

[1]E. A. Silinsh, *Organic Molecular Crystals* (Springer-Verlag, Berlin, 1980).

[2]M. Pope and C. E. Swenberg, *Electronic Processes in Organic Crystals* (Oxford University Press, Oxford, 1982).

[3]R. S. Berry, J. Jortner, J. C. Mackie, E. S. Pysh, and S. A. Rice, J. Chem. Phys. **42**, 1535 (1965).

[4]S. C. Abbi and D. M. Hanson, J. Chem. Phys. **60**, 319 (1974).

[5]L. Sebastian, G. Weiser, and H. Bässler, Chem. Phys. **61**, 125 (1981).

[6]P. J. Bounds and W. Siebrand, Chem. Phys. Lett. **75**, 414 (1980).

[7]Z. Shen, P. E. Burrows, S. R. Forrest, M. Ziari, and W. H. Steier (unpublished).

[8]F. F. So, S. R. Forrest, Y. Q. Shi, and W. H. Steier, Appl. Phys. Lett. **56**, 674 (1990).

[9]F. F. So and S. R. Forrest, Phys. Rev. Lett. **66**, 2649 (1991).

[10]E. I. Haskal, Y. Zhang, P. E. Burrows, and S. R. Forrest, Chem. Phys. Lett. **219**, 325 (1994).

[11]A. J. Lovinger, S. R. Forrest, M. L. Kaplan, P. H. Schmidt, and T. Venkatesan, J. Appl. Phys. **55**, 476 (1984).

[12]S. R. Forrest, M. L. Kaplan, and P. H. Schmidt, J. Appl.

Phys. **55**, 1492 (1984).
[13]D. Y. Zang, F. F. So, and S. R. Forrest, Appl. Phys. Lett. **59**, 823 (1991).
[14]S. R. Forrest, P. E. Burrows, E. I. Haskal, and F. F. So, Phys. Rev. B **49**, 11 309 (1994).
[15]Aldrich Chemical Company, Milwaukee, WI.
[16]T. Maki and H. Hashimoto, Bull. Chem. Soc. Jpn. **25**, 411 (1952).
[17]F. Gutmann and L. E. Lyons, *Organic Semiconductors* (Wiley, New York, 1967).
[18]P. Fenter, P. E. Burrows, P. Eisenberger, and S. R. Forrest (unpublished).
[19]E. I. Haskal, F. F. So, P. E. Burrows, and S. R. Forrest, Appl. Phys. Lett. **60**, 3223 (1992); P. E. Burrows and S. R. Forrest, *ibid.* **62**, 3102 (1993).
[20]S. R. Forrest and Y. Zhang, Phys. Rev. B **49**, 11 297 (1994).
[21]T. Takase and M. Kotani, J. Chem. Phys. **90**, 2134 (1988).
[22]S. R. Forrest, M. L. Kaplan, and P. H. Schmidt, J. Appl. Phys. **56**, 543 (1984).
[23]A lower-energy feature at $\lambda=585$ nm has also been found in the photocurrent spectrum of PTCDA photoconductors. We tentatively assign this feature to a Frenkel exciton in PTCDA, where the Frenkel exciton is typically at a lower energy than the CT excitons which are the subject of this study.
[24]D. Y. Zang and S. R. Forrest, Appl. Phys. Lett. **60**, 189 (1992).
[25]C. Weisbuch, R. Dingle, A. C. Gossard, and W. Wiegmann, Solid State Commun. **38**, 709 (1981).
[26]F. F. So, Ph.D. thesis, University of Southern California, Los Angeles, CA, 1991; Y. Ohmori, A. Fujii, M. Uchida, C. Morishima, and K. Yoshino, Appl. Phys. Lett. **63**, 1871 (1993).
[27]H. Jung, A. Fischer, and K. Ploog, Appl. Phys. A **33**, 97 (1984).
[28]J. F. Lam, S. R. Forrest, and G. L. Tangonan, Phys. Rev. Lett. **66**, 1614 (1991).
[29]C. V. Shank, E. P. Ippen, and O. Teschke, Chem. Phys. Lett. **45**, 291 (1977).
[30]V. L. Broude, E. I. Rashba, and E. F. Sheka, *Spectroscopy of Molecular Excitons* (Springer-Verlag, Berlin, 1985).
[31]E. F. McCoy and I. G. Ross, Aust. J. Chem. **15**, 573 (1962).
[32]I. B. Berlman, J. Phys. Chem. **74**, 3085 (1970).
[33]J. Takada, H. Awaji, M. Koshioka, W. A. Nevin, M. Imanishi, and N. Fukada, J. Appl. Phys. **75**, 4055 (1994).
[34]Here, the first moment of the spectrum is defined as $\bar{\omega}^{(1)}=\int \omega I(\omega)d\omega / \int I(\omega)d\omega$, where $I(\omega)$ is the fluorescence intensity at ω.
[35]D. Haarer, Chem. Phys. Lett. **27**, 91 (1974).
[36]R. W. Munn and W. Siebrand, J. Chem. Phys. **52**, 47 (1970).
[37]S. R. Forrest, L. Y. Leu, F. F. So, and W. Y. Yoon, J. Appl. Phys. **66**, 5908 (1989).
[38]V. M. Agranovich, R. D. Atanasov, and G. F. Bassani, Chem. Phys. Lett. **199**, 621 (1992).
[39]V. M. Agranovich, Phys. Scr. **149**, 699 (1993).

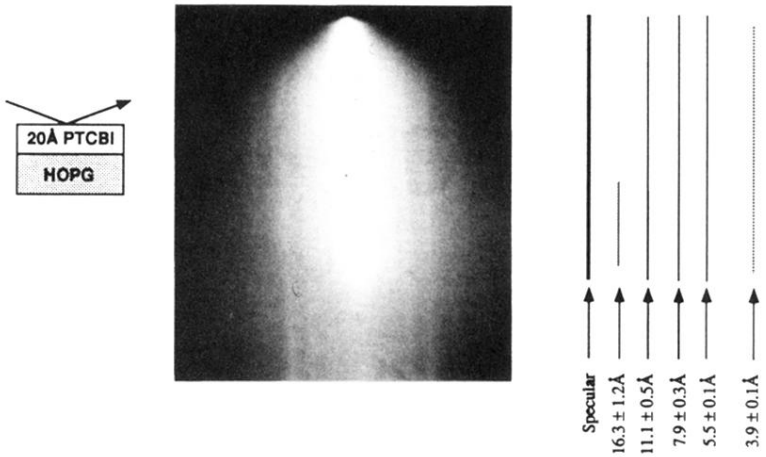

FIG. 2. Reflection high-energy electron-diffraction pattern of an OMBD-grown 20 Å PTCBI layer on highly oriented pyrolitic graphite. Streaks are labeled with their corresponding lattice dimensions.